Computers in Biology and Medicine 196 (2025) 110676

Contents lists available at ScienceDirect

Computers in Biology and Medicine

journal homepage: www.elsevier.com/locate/compbiomed

Automatic CNN-based 3D/2D non-rigid registration platform for fast 3D femur reconstruction and clinical 3D measurements from Bi-planar radiographs

Nahid Babazadeh Khameneh [a,b,*], Thierry Cresson [a,b], Frédéric Lavoie [c], Jacques de Guise [a,b], Carlos Vázquez [a]

[a] Laboratoire d'Innovation Ouverte (LIO), École de technologie supérieure, Montréal, Québec, Canada
[b] Centre de recherche du CHUM, Montréal, Québec, Canada
[c] Centre Hospitalier Université de Montréal (CHUM), Montréal, Québec, Canada

ARTICLE INFO

Keywords:
CNN cascade-based 3D/2D non-rigid registration platform
Fully automatic
Fast personalized 3D femur reconstruction
Clinical 3D measurement
2D bi-planar radiographs

ABSTRACT

Purpose: This paper presents an automatic 3D/2D non-rigid registration method for fast 3D reconstruction and clinical measurements of the femur.

Approach: The proposed CNN cascade-based 3D/2D registration platform comprises three major steps to fit a generic 3D femur model into 2D bi-planar EOS® radiographs: 1) Pose estimation ($\boldsymbol{CNN_{Pose}}$)- a combination of Principal Component Analysis (PCA) and CNN-based 3D/2D similarity registration; 2) 3D shape deformation ($\boldsymbol{CNN_{Shape}}$)- a CNN-based 3D displacement estimation of handles followed by Moving Least Square (MLS) shape deformation to extend an as-rigid-as-possible deformation to the entire bone, 3) 3D scale deformation ($\boldsymbol{CNN_{Scale}}$)- a CNN-based 3D scale ratio estimation of handles followed by MLS-based model rescaling.

Results: The accuracy of the method is evaluated in comparison to, first, a clinically proved semi-automatic method on 15 patients, and second, Computerized Tomography CT scans of five new patients. In the first validation, the mean ± standard deviation (STD) of the Root Mean Square of point-to-surface distance (RMS-P2S) error is 0.88± 0.29 mm. For the second validation, the mean± STD of RMS-P2S error is 2.70± 0.39 mm. Four clinical measurements of the reconstructed 3D femurs are computed and compared with the first validation set. For each clinical measurement, the Mean Absolute Errors (MAE) is below 1 mm or 1°.

Conclusions: The presented automatic CNN cascade-based framework efficiently registers the generic 3D femur models into bi-planar radiographs. The CNN-based 3D handles displacement and scale estimation eliminates manual-annotations and user-interventions for MLS deformation while maintaining accuracy and speed. This system is applicable for other bones such as the tibia.

1. Introduction

Clinical 3D geometric measurements of the lower limb bones such as the femur, are crucial in orthopedic pre-operative planning and patient follow-up [1,2]. In clinical routine, the personalized 3D model reconstruction of the femur is a useful tool for physicians to quantify clinical 3D geometric measurements such as the size, curvatures, orientations, and femoral torsion ([3]; Reyneke et al., 20219). 2D bi-planar radiographs-based 3D femur reconstruction methods provides an efficient alternative to Computerized Tomography (CT) [3–5] for orthopedic surgical planning [6] and patient follow-up [7].

Personalized 3D bone reconstruction from 2D bi-planar radiographs has been investigated over the last two decades [3–5]. In this 3D reconstruction process, 3D/2D registration is usually essential to establish a geometrical relationship between a known prior 3D model and a patient's 2D bi-planar radiographs [5,8,9]. This registration process, which includes the 3D pose and the 3D shape estimation of bone structures from only two 2D projections, is highly complex due to information loss during 2D projection of 3D bones and to the need to solve an inverse problem using 2D projected sparse data [8–11]. Semi-automatic methods, such as the one employed by the EOS® 3D model reconstruction system [10], require the manual intervention of an

* Corresponding author. Laboratoire d'Innovation Ouverte (LIO), École de technologie supérieure, Montréal, Québec, Canada.
E-mail addresses: nahid.babazadeh-khameneh.1@ens.etsmtl.ca (N.B. Khameneh), carlos.vazquez@etsmtl.ca (C. Vázquez).

https://doi.org/10.1016/j.compbiomed.2025.110676
Received 23 January 2025; Received in revised form 8 June 2025; Accepted 24 June 2025
Available online 3 July 2025

operator for pose initialization and scale and shape adjustment of the 3D model to images [8,10–16]. These manual interventions impact the accuracy, time efficiency and reproducibility of the different approaches [10]. Recently, efforts have been deployed to remove any intervention by the operator [9] and improve the time efficiency [17] of the registration approaches. Although full automation is highly desired, there is always the potential for errors in the 3D reconstruction process that need to be manually corrected to facilitate deployment in clinical practice [10–16,18]. The current semi-automatic EOS® 3D femur reconstruction method and 3D geometric measurements quantification system [10], which is already integrated in the existing and established commercial SterEOS software tool [19], has been validated by clinicians, and has reached reliable and significant accuracy allowing it to be used as a very useful diagnostic tool assisting physicians in assessing lower limbs deformity [19–22]. This method uses the Moving Least Square (MLS) deformation approach to fit a generic 3D femur model into the patient's 2D bi-planar radiographs and allows physicians, if required, to easily refine the reconstructed 3D model. However, this semi-automatic approach suffers from lack of time efficiency and reproducibility [10, 19].

To meet this need, we automate the current semi-automatic EOS® 3D model reconstruction system, which is already integrated in a clinical application. The present paper proposes an automatic 3D/2D non-rigid registration method to fit a generic 3D femur model into the patient's EOS® bi-planar radiographs to accurately assess clinical 3D geometric parameters in a time-efficient manner. This method is easily adaptable by clinicians and allows them to quickly and easily adjust the reconstructed 3D femur.

The proposed automatic 3D/2D non-rigid registration framework combines deep Convolutional Neural Networks (CNN) cascade-based registration models and the Moving Least Square (MLS) deformation to fit the generic 3D femur model into the patient's 2D bi-planar radiographs. In Sec.2, related work is introduced. Section 3 presents the proposed automatic 3D/2D registration workflow. Section 4 describes data preparations, followed by the experimental setup in Sec. 5. Results are depicted in Sec. 6. A discussion is being carried out in Sec. 7. Conclusions are outlined in Sec. 8.

2. Related work

In 2D radiograph-based 3D femur reconstruction, state-of-the-art 3D/2D registration methods range from semi-automatic [8,10,11] to automatic [9]. In the 3D model reconstruction, a known prior 3D model such as a CT-scan or Magnetic Resonance Imaging (MRI)-based 3D model [7,23], a statistical shape model (SSM) [8,11,16,24], or a generic template model [9,10,20] could be registered into the patient's calibrated 2D bi-planar radiographs. The choice of the 3D prior model drives the 3D bone reconstruction process. In SSM-based 3D femur reconstruction, Principal Component Analysis (PCA) is a very useful and popular method used to handle and regularize 3D shape deformation [8, 12,16,18,24]. Unlike PCA-based 3D reconstructions, which require a training process and the collection of a CT-scan-based data set [8,12,16, 18,24], interpolation-based methods [10,25] construct personalized 3D bone models from a single CT-scan-based reconstructed generic 3D model of the target structure without statistical knowledge of the population. In contrast to PCA-based methods, which globally constrain 3D shape deformation to the training population, an interpolation-based method using a generic 3D model provides flexible and local 3D shape and scale deformations [10,25].

In semi-automatic 3D/2D registration methods, an operator manually initializes the prior 3D model close to the optimal position in the patient's 2D bi-planar radiograph reference space [8,10,11,16]. Then, to optimize the 3D model's shape and scale, a (dis)similarity measurement (matching) term as an objective function is defined and iteratively optimized over geometric [8,10,11,14,16,26], intensity [18,24] or hybrid [9,19,35] features. Geometric feature-based methods are limited to establishing accurate 2D [16] or 3D correspondences such as edges, non-stereo corresponding contours [14], and salient landmarks [11] between the 3D model and the target bone structures appearing in 2D radiographs. These approaches in Ref. [8,10,11,14,16] suffer from a lack of reproducibility and robustness. Iterative optimization of an intensity-based matching term is highly non-convex over registration parameters, and so, the registration task is prone to getting trapped in a local optimal when the starting position is far from the optimal one, and in addition, it suffers from a lack of robustness [27–29]. To address these limitations, hybrid feature-based methods use geometric features for a coarse 3D pose initialization close to the optimal position, and then use intensity features for a fine registration [9].

A semi-automatic 3D reconstruction method [10,22] is already used in clinical routines as it provides a user-friendly 3D model adjustment. An interpolation-based method [10] uses a small set of defined stereo and non-stereo corresponding (NSC) control points on the generic 3D model of the target bone to manipulate and control 3D shape deformation using the MLS method. The MLS deformation drives a constrained and as-rigid-as-possible local 3D shape deformation on a small set of 3D handles and avoids undesirable distortion in the entire generic 3D model, which is suitable for a fast 3D bone reconstruction [10,25]. The MLS deformation method does not take into account any statistical shape information about the 3D model and it is an appropriate and user friendly approach for clinical 3D geometrical parameters assessment [10]. In Ref. [10], a small set of 17 handles are manually displaced over the whole femur by an operator, and the reported mean reconstruction time for both lower limbs is 10 min, with CPU computation. However, the 3D femur reconstruction method in Ref. [10] suffers from operator intervention, a lack of reproducibility, and high time consumption. In contrast, Cresson e al. [25] proposes a contour-based iterative optimization of the 17 MLS handles for 3D femur reconstruction. However [25], suffers from manual initialization. In Ref. [9], the interpolation-based free-form deformation (FFD) is used for control point-based 3D shape deformation. In contrast to MLS deformation, which allows physicians to easily refine the 3D shape, a large set of 3D control points (88) are uniformly distributed over the entire 3D volumetric template, making any further adjustments almost impossible. This makes it hard to deploy the automatic method of [9] in clinical routine. Moreover, in rigid bone deformation, FFD is likely to produce undesirable distortion and needs strong regularization [9]. Of note, MLS deformation could avoid such undesirable distortion [30]. Recently, emerging machine learning (ML)-and deep learning (DL)-based approaches have contributed significantly to reduce operator interventions and manual initialization to facilitate the automation of 3D/2D registration [31]. The work in Ref. [9] proposes an automatic 3D/2D similarity registration of the proximal femur by using an automatic machine learning-based segmentation, via random forest regression, of the target bone structure to initialize a template 3D model without user interventions. In an automatic 3D/2D rigid registration of a Transesophageal Echocardiography (TEE) probe [26], proposes an automatic 3D pose initialization via the marginal space learning method. The deep CNN performs very well in learning the non-linearity of the mapping function between input image features and transformation parameters [27–29,31]. In contrast to Ref. [9] and [46], a deep learning-based optimization method [27–29] overcomes the limitations of non-convex intensity-based (dis)similarity term optimization. In Ref. [27], known rigid 3D objects such as the knee prosthesis 3D model, the TEE probe, and a tooth implant are registered into the patient's 2D frontal radiograph. Hierarchical regression models based on a CNN are trained to regress six rigid transformation parameters (6DOF) from local intensity residual inputs between Digitally Reconstructed Radiographs (DRRs) of TEE and X-ray images [27]. The proposed deep learning-based registration method shows enough robustness to produce the same registration results from different starting positions [27]. In Ref. [29], to improve the accuracy and capture the TEE probe tracking range of [27], a coarse-to-fine strategy is proposed for CNN-based 3D/2D rigid

registration. The authors refine the accuracy and the capture range of the registration by applying a second registration step on the output of the coarse step [29]. In CNN-based non-rigid registrations [32,33], present unsupervised VoxelMorph and TransMorph models, respectively, for 3D MRI brain deformation. In VoxelMorph and TransMorph models, an unsupervised atlas-based registration works without ground truths and the reference image is an atlas, which is an average volume obtained from repeatedly registration of brain volumes in the population. The VoxelMorph and TransMorph models combine CNN and spatial transformation to deform 3D MRI volumes. First, a CNN-based model with U-Net architecture learns to estimate deformation field from input source and reference images. Second, following CNN-based model, an spatial transformation function uses CNN-based estimated deformation filed to interpolate new voxel locations based on the eight neighbors. Then, the deformed image backpropagated to the model until convergence. However, TransMorph model uses U-Net architecture with transformed-based encoder to capture long-range relationships in registration [33].

In automatic and fast 3D bone reconstruction applications, recent developments in CNN-based methods show promising results on assigned tasks without user interventions [17,34]. Over the last decade, in many 2D radiograph-based 3D model reconstruction applications, DL-based methods have been useful tools for automatic and fast non-rigid registration [17,31]. For instance, in fully automatic 2D bi-planar radiographs-based 3D spine reconstruction [17], a CNN-based regression model successfully estimates 3D displacements of corresponding stereo landmarks and the vertebral body center (VBC) from input (frontal + lateral) local patches. In an automatic 3D knee bone reconstruction from 2D bi-planar radiographs [34], supervised and non-supervised CNN-based models are used for 3D segmentation of the knee bone. The CNN learns to directly reconstruct 3D models of the knee from input DRRs rendered from CT-scans. Finally, an MLS-based 3D femur reconstruction method is integrated in the commercial SterEOS software tool [10] and is currently used in clinical routine to assess clinical 3D geometric parameters of the bone structure. Although this semi-automatic approach provides physicians with an easy and user-friendly way to manually carry out adjustments to correct potential 3D reconstruction errors to get better assessment of clinical 3D parameters, it has nonetheless certain limitations, such as dependency on the operator's skill, limited reproducibility, and high time consumption [10]. This semi-automatic 3D femur reconstruction and clinical 3D parameters measurement approach could be automated to remove its current limitations. To this end, the present paper automates MLS-based 3D femur reconstruction method [10], integrated in the existing and established semi-automatic commercial SterEOS software tool [19], with the ability to easily adjust, if required, the reconstructed 3D model via a small number of MLS handles. We propose a CNN cascade-based 3D/2D non-rigid registration which automatically estimates 3D displacements and scale ratios of MLS handles. In clinical 3D geometrical parameters measurement, the contribution of this work merges the estimation of CNN-based handle 3D displacements and scale ratios with MLS deformation handles to automate the 3D/2D non-rigid registration process. The main benefit of this automated approach is its ease of adoption by clinicians, and seamlessly integrating with existing commercial SterEOS software [19] by automatically estimating 3D handles. Compared to the current semi-automatic EOS® 3D femur reconstruction method [10] and 3D geometric measurements quantification system [10,19], this work achieved good results.

3. Automatic 3D/2D registration

The proposed CNN cascade-based 3D/2D registration platform automatically fits $(\boldsymbol{M_g})$, the generic 3D model of the target 3D bone structure, into $(\boldsymbol{F})$, which is the patient's 3D bone, using 2D bi-planar radiographs, as Eq. (1):

$$(\boldsymbol{F}) = U_{Scale} \circ \left(U_{Shape} \circ \left(U_{Pose} \circ (\boldsymbol{M_g})\right)\right) \quad (1)$$

The CNN cascade-based 3D/2D registration framework (Fig. 1) consecutively uses three CNN-based regression models, CNN_{Pose}, CNN_{Shape}, and CNN_{Scale} to fit $(\boldsymbol{M_g})$ into $(\boldsymbol{F})$ via two main stages:

(1) 3D/2D similarity registration (U_{Pose}): in a coarse-to-fine 3D/2D similarity registration, a PCA-based alignment [29] is used to coarsely initialize the pose of the generic 3D model of the femur [35]. The PCA is applied on CNN-based segmented masks of the detected femur in the EOS® 2D bi-planar radiographs to recover 3D similarity transformation parameters, including translation, rotation and scale [20]. In the refining step, CNN-based regression models are trained to obtain more accurate 3D pose parameters [35].

(2) 3D/2D non-rigid registration, including local 3D shape deformation (U_{Shape}) and local 3D scale deformation (U_{Scale}): to deform the local shape of the registered 3D femur model, CNN-based regression models are trained to find 3D displacements of a small number of 3D handles pre-defined on the femur. Following the computation of the new positions of 3D handles, an MLS deformation is applied to obtain a 3D model better adjusted to the radiographs without any user interactions. To optimize the local 3D scale corresponding to each handle, CNN-based regression models are trained to estimate the local 3D scale ratios corresponding to the said handles. Then, the MLS method is used to compute 3D rescaling fields and extend the scales to the entire 3D femur.

To begin with the methodology, subsection 3.1 introduces the generic 3D model and the 3D coordinate system, which will be used in all methodology subsections. subsection 3.1.1 presents MLS deformation method. Section 3.2 presents the structure of the convolutional neural network models that we train for CNN cascade-based 3D/2D registration framework. Section 3.3 describes an automatic CNN-based similarity registration (U_{Pose}). Section 3.4 presents 3D/2D automatic non-rigid registration process through two main subsections 3.4.1 and 3.4.2. subsection 3.4.1 describes automatic 3D shape deformation process (U_{Shape}) through subsections 3.4.1.1 and 3.4.1.2 for CNN-based 3D displacement estimation and automatic 3D shape deformation, respectively. Finally, subsection 3.4.2 presents automatic 3D scale deformation process (U_{Scale}) through subsections 3.4.2.1 and 3.4.2.2 for CNN-based 3D scale ratios estimation and automatic 3D scaling, respectively.

3.1. Deformable generic 3D model and 3D coordinate system

To begin, the position of the generic 3D model $(\boldsymbol{M_g})$ and the patient's bone structure are defined with respect to the origin of the 3D referential of the EOS cabin system $(0,0,0)$, (Fig. 2). We use the same generic 3D model $(\boldsymbol{M_g})$ constructed by Ref. [10], which is a CT-scan-based reconstructed 3D surface mesh of the left femur. A set of 17 3D handles recorded as $\boldsymbol{CP} = \{\boldsymbol{cp}_i \in \mathbb{R}^3 | i = 1, \cdots, 17\}$ are defined beforehand by Ref. [10] on the generic 3D model $(\boldsymbol{M_g})$, (Fig. 2), to manipulate and control the 3D bone shape deformation. Of the 17 3D handles, $\boldsymbol{cp}_1$ to $\boldsymbol{cp}_{12}$ are 3D point handles with uniform scale, and are located on the proximal and distal femoral regions. $\boldsymbol{cp}_{13}$ to $\boldsymbol{cp}_{17}$ are the spline handles with non-uniform scale and are located on the femoral diaphysis. The latter handles are more appropriate for depicting the 3D shape deformation of the femoral diaphysis [10]. The 3D mesh $(\boldsymbol{M_g})$ is constructed by a set of 3D vertices $(\boldsymbol{V_g})$, and each $\boldsymbol{cp}_i$ is surrounded by a corresponding subset of vertices called $\boldsymbol{v}_i$.

3.1.1. MLS deformation of generic 3D model

To deform the generic 3D model, which is controlled by 17 handles,

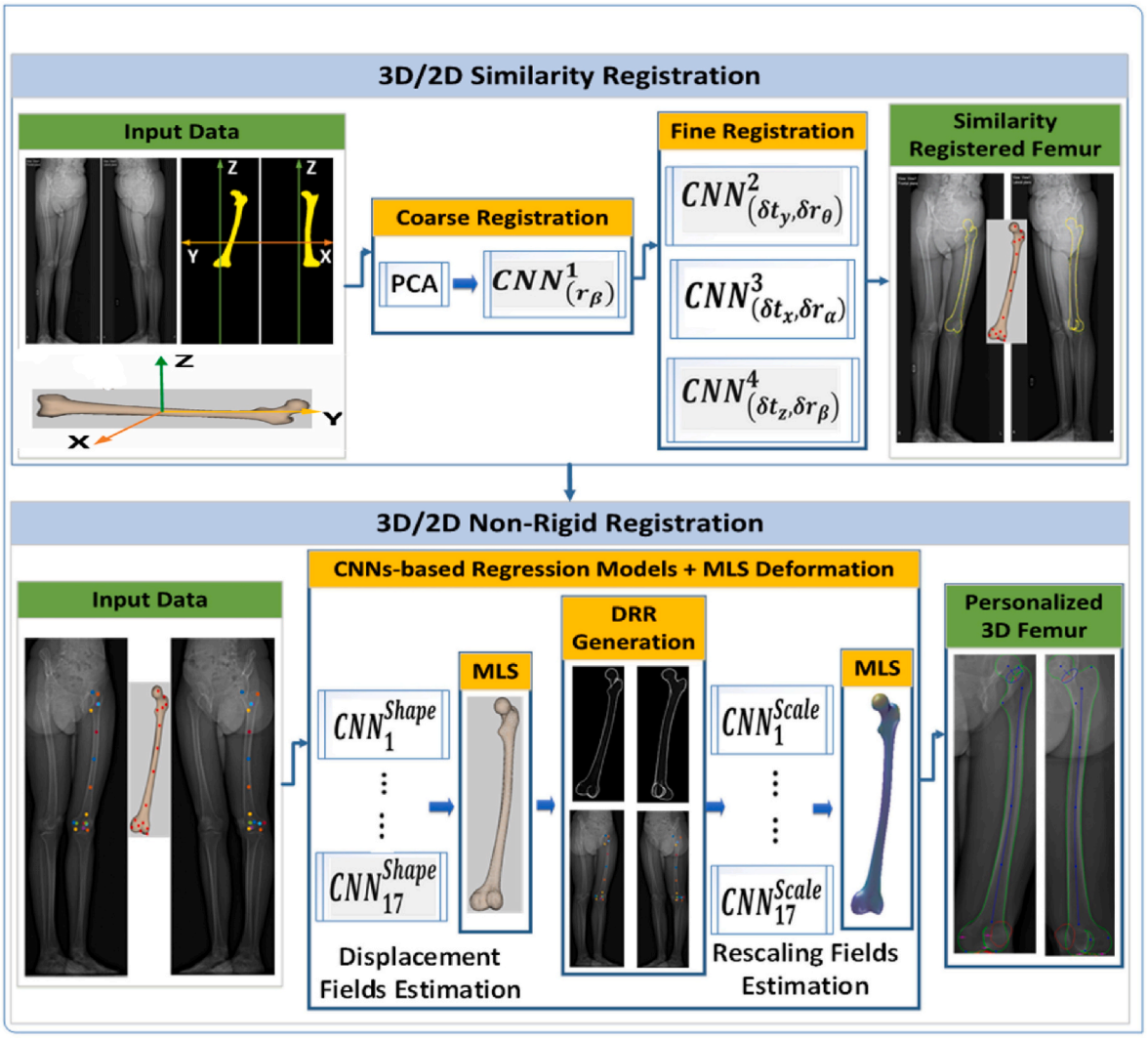

Fig. 1. Automatic 3D/2D registration framework in two main stages: (1) 3D/2D similarity registration (top row), and (2) 3D/2D non-rigid registration (bottom row).

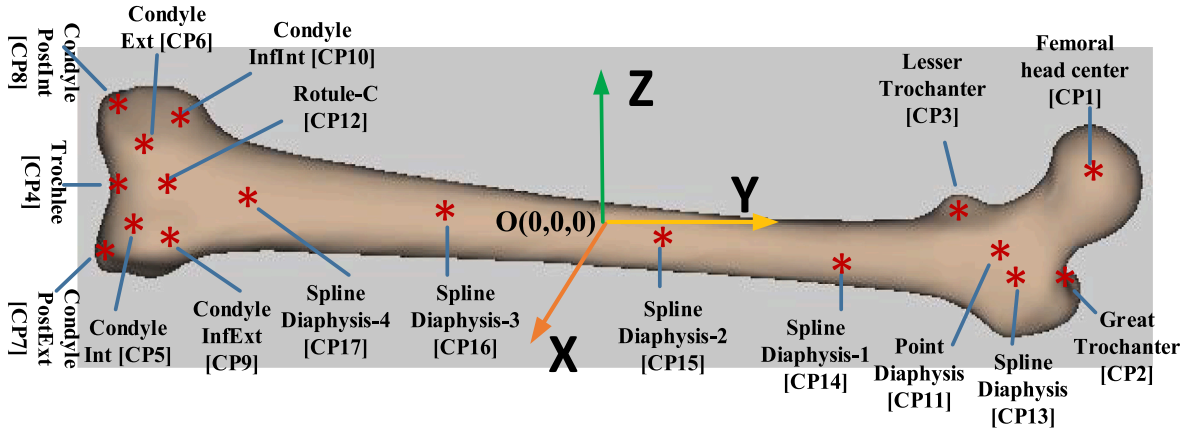

Fig. 2. Femoral shape description with 17 3D handles at the origin of the 3D referential of the EOS® cabin system.

we apply the MLS deformation method [10,22]. Given two sets of 3D positions for 17 handles, $\boldsymbol{CP}^T$ (source) and $\boldsymbol{CP}'$ (reference), the MLS deformation method [10,25] locally computes the new positions of the corresponding subset of 3D vertices, $\boldsymbol{v}_i$ of $\left(\boldsymbol{M}_g^T\right)$. The Weighted Least Squares (WLS) optimization, as Eq. (2), provides a locally constrained shape deformation based on a weight function, w_i, as [10,25]:

$$\widehat{D}_{\boldsymbol{v}_i} = \underset{D_{\boldsymbol{v}_i}}{argmin}\left(w_i \cdot \left\|\boldsymbol{cp}' - \boldsymbol{D}_{\boldsymbol{v}}\left(\boldsymbol{cp}^T\right)\right\|^2\right), \forall \boldsymbol{v}_i \in \left(\boldsymbol{V}_g^T\right), \tag{2}$$

$$w_i = \frac{1}{d(\boldsymbol{cp}_i^T, \boldsymbol{v}_i)^{2\alpha}}$$

Where $\widehat{\boldsymbol{D}}_{\boldsymbol{v}_i}$ is an optimal similarity transformation associated with $\boldsymbol{cp}_i^T$ and its corresponding subset of vertices $\boldsymbol{v}_i$ and $d(\cdot,\cdot)$ is the Euclidean distance between each vertex of the subset $\boldsymbol{v}_i$ and $\boldsymbol{cp}_i^T$. The function $d(\cdot,\cdot)$ measures the distance between each v_i on $\left(\boldsymbol{M}_g^T\right)$ and the handle $\boldsymbol{cp}_i^T$ with Euclidean norm. The impact of $d(\cdot,\cdot)$ on the displacement field of v is controlled by the parameter $\alpha > 0$. The parameter $\alpha > 0$ controls the effect of distant handles on the deformation of the subset of vertices $\boldsymbol{v_i}$. For each handle, the closest vertices gain more weight and are affected more.

The optimal similarity transformation $\widehat{\boldsymbol{D}}_{\boldsymbol{v}_i}$ is found using singular value decomposition [36] (SVD) by solving a least squares regression between the source ($\boldsymbol{CP}^T$) and target ($\boldsymbol{CP}'$) 3D handles. To avoid undesirable distortion and non-uniform scaling, for each handle $\boldsymbol{CP}_i^T$, $\widehat{\boldsymbol{D}}_{\boldsymbol{v}_i}$ is restricted to a similarity transformation as Eq. (3):

$$\boldsymbol{CP}_i^T \rightarrow \widehat{\boldsymbol{D}}_{\boldsymbol{v}_i}\left(\boldsymbol{CP}_i^T\right) = sc_{Global}\boldsymbol{r}_i\boldsymbol{CP}_i^T + \boldsymbol{t}_i \tag{3}$$

Where SC_{Global} is the uniform global scaling and $\boldsymbol{r}_i$ is a local 3D rotation followed by a local 3D translation t_i associated with $\boldsymbol{CP}_i^T$. For each handle $\boldsymbol{cp}_i^T$, we transform the corresponding subset of vertices $\boldsymbol{v}_i$ with $\widehat{\boldsymbol{D}}_{\boldsymbol{v}_i}$ to obtain a locally constrained and smooth 3D shape deformation of the 3D model $\left(\boldsymbol{M}_g^T\right)$. The deformed 3D model $\left(\boldsymbol{M}_g^{\hat{D}_v(T)}\right)$ is used as an input for the next local 3D scale ratio estimation.

3.2. Convolutional Neural Networks structure

A CNN cascade-based 3D/2D registration framework comprises 38 CNN-based regression models: four for (U_{Pose}), 17 for (U_{Shape}) and 17 for (U_{Scale}), corresponding to $\boldsymbol{CP}^T$. The regression models for (U_{Pose}) are multi-channel CNN, as described in Ref. [35], while those for (U_{Shape}) and (U_{Scale}) are bi-channel CNN, which are used to estimate the handles' 3D displacements and 3D scale ratios, respectively, and have the same structure as [35]. For CNN_{Shape} and CNN_{Scale} (Fig. 3), shows the structure of a bi-channel CNN-based regression model corresponding to bi-planar input patches. Each CNN channel is constructed from two convolutional layers followed by drop-out layers, two max pooling layers, and a fully connected layer. The extracted feature maps from each CNN channel are concatenated and passed to another fully connected layer. The next fully connected layer is the output layer. Each CNN-based regression model is trained to minimize the Euclidean loss as an objective function, as Eq. (4):

$$\psi = \frac{1}{n}\sum_{j=1}^{n}\left\|g_j - y_j\right\|_2^2 \tag{4}$$

Where n is the number of training samples, g_j is the known target, and y_j is the estimated output

for the j^{th} training sample. For Sec.3.3 (U_{Pose}), 3.4.1 (U_{Shape}), and 3.4.2 (U_{Scale}), g_j and y_j are the target and estimated 3D pose parameter residual, 3D displacement, and 3D scale ratio, respectively. The inputs for (U_{Pose}), (U_{Shape}), and (U_{Scale}) are the local intensity (or residual) patches described in Sec.3.4.1 and 3.4.2, respectively.

3.3. Automatic 3D/2D similarity registration (U_{Pose})

The generic 3D model $(\boldsymbol{M}_g)$ is initialized in the patient's EOS 3D radiograph space and registered into $(\boldsymbol{F})$, the projection of the patient's bone of interest in 2D bi-planar radiographs, using the fully automatic CNN-based method previously presented in Ref. [35]. We use the coarse-to-fine 3D/2D similarity registration (U_{Pose}) method to estimate a seven-degrees-of-freedom (7DOF) 3D pose, and the isotropic scale parameters, $T(t_x, t_y, t_z, r_\theta, r_\alpha, r_\beta, s)$, to align $(\boldsymbol{M}_g)$ into $(\boldsymbol{F})$. To roughly locate the 3D bone, first, a PCA-based registration [45] is used to estimate $(t_x, t_y, t_z, r_\theta, r_\alpha, s)$, following an automatic CNN-based semantic segmentation of the target bone [37]. Secondly, a CNN-based regression model [20], $CNN^1_{(r_\beta)}$, is trained to estimate (r_β). In the fine step to refine the

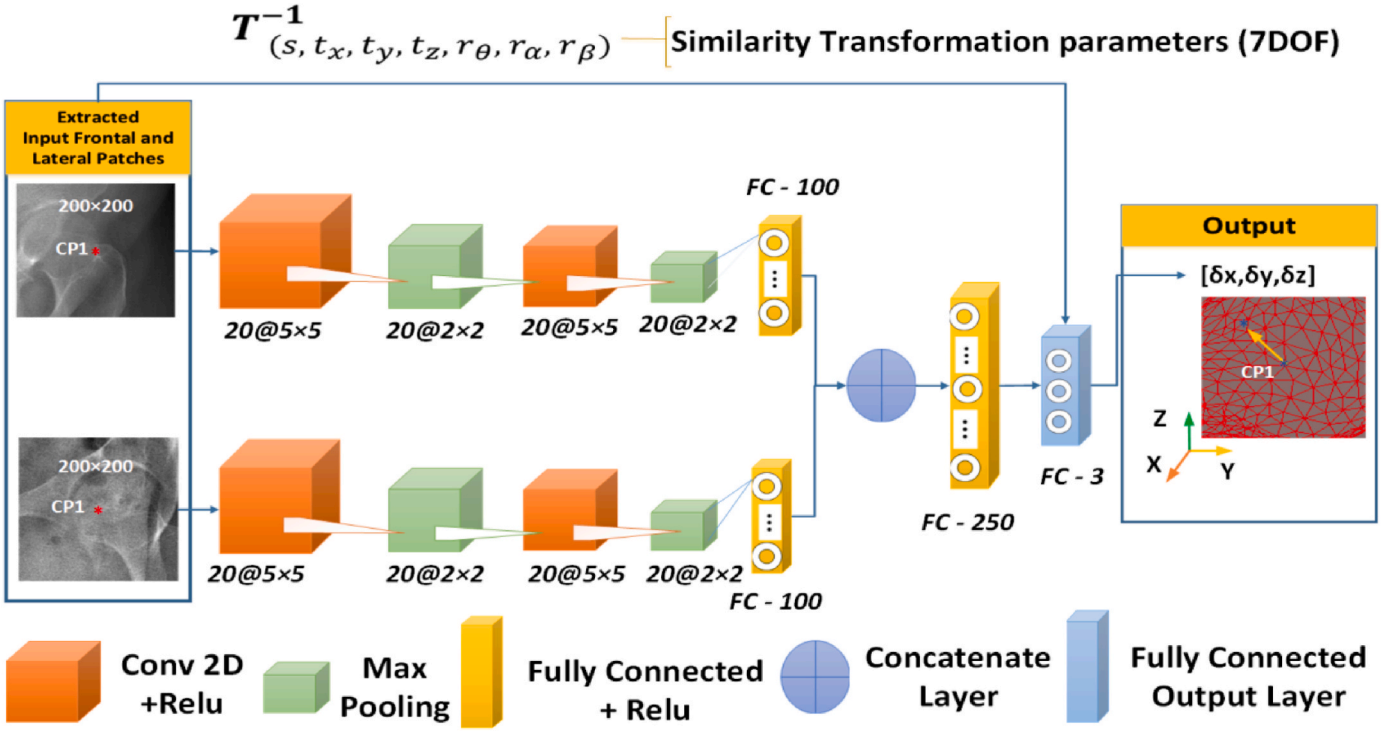

Fig. 3. Bi-channel CNN-based regression model structure corresponding to the 3D handle $\boldsymbol{cp}_1$.

transformation parameters, three CNN-based regression models, $CNN^2_{(\delta t_y, \delta r_\theta)}$, $CNN^3_{(\delta t_x, \delta r_\alpha)}$, and $CNN^4_{(\delta t_z, \delta r_\beta)}$, are trained from bi-planar pose-invariant local intensity residuals, centered at the 2D projections of automatically computed six pose-invariant points of

the left femur (Fig. 4), to refine 3D pose residuals and reach the most accurate 3D position [35]. Then, $(\boldsymbol{M}_g)$ is transformed with the computed transformation T to obtain $\left(\boldsymbol{M}_g^T\right)$, which is used as input for the automatic 3D/2D non-rigid registration.

3.4. Automatic 3D/2D non-rigid registration

3.4.1. *Automatic 3D shape deformation* (U_{Shape})

To perform a personalized and as-rigid-as-possible local 3D bone deformation, we propose a fast and automatic handle-based 3D/2D non-rigid registration algorithm combined with MLS deformation [10,25]. In (U_{Shape}), first, CNN-based regression models are trained to estimate the 3D displacements of a small set of 17 handles of the generic 3D model (Sec.3.1, Fig. 2). Given the new positions of the handles, we apply MLS deformation (Sec.3.1.1) without any user interventions.

3.4.1.1. CNN-based 3D displacements estimation. To deform the 3D model $\left(\boldsymbol{M}_g^T\right)$, we estimate 3D displacements of the set of 17 handles, $\boldsymbol{CP}$ (Fig. 2). A set of 17 CNN-based regressors, $\boldsymbol{CNNs}^{\boldsymbol{Shape}} = \left\{CNN_i^{Shape} \middle| i = 1, \cdots, 17\right\}$, are independently trained to directly estimate the handles' 3D displacements between the current and target positions, $\boldsymbol{\Delta}_{\text{xyz}} = \{(\delta x, \delta y, \delta z)_i | i = 1, \ldots, 17\}$. The inputs of each CNN_i^{Shape} are bi-planar local intensity patches (LIs) (Sec.3.2) extracted from the patient's 2D bi-planar radiographs (I_F, I_L) at a size of 200 × 200 pixels. The input LIs of CNN_i^{Shape} are centered at 2D frontal and lateral projections of the 3D handles, $\boldsymbol{cp}_i{}^T$, transformed using the similarity transformation T previously estimated in Sec.3.3. Each CNN_i^{Shape} (Fig. 3) learns a mapping function f_1 between the input LIs and corresponding 3D displacements $(\delta x, \delta y, \delta z)_i$, as Eq. (5):

$$f_1\left(LIs\left(\boldsymbol{cp}_i^T, (I_F, I_L)\right), \left(\boldsymbol{M}_g^T\right)\right)_i = (\delta x, \delta y, \delta z)_i \tag{5}$$

Afterward, $\boldsymbol{CP}'$ is computed as a set of new positions for $\boldsymbol{CP}^T$, as Eq. (6):

$$\boldsymbol{CP}' = \boldsymbol{CP}^T + \boldsymbol{\Delta}_{\text{xyz}} \tag{6}$$

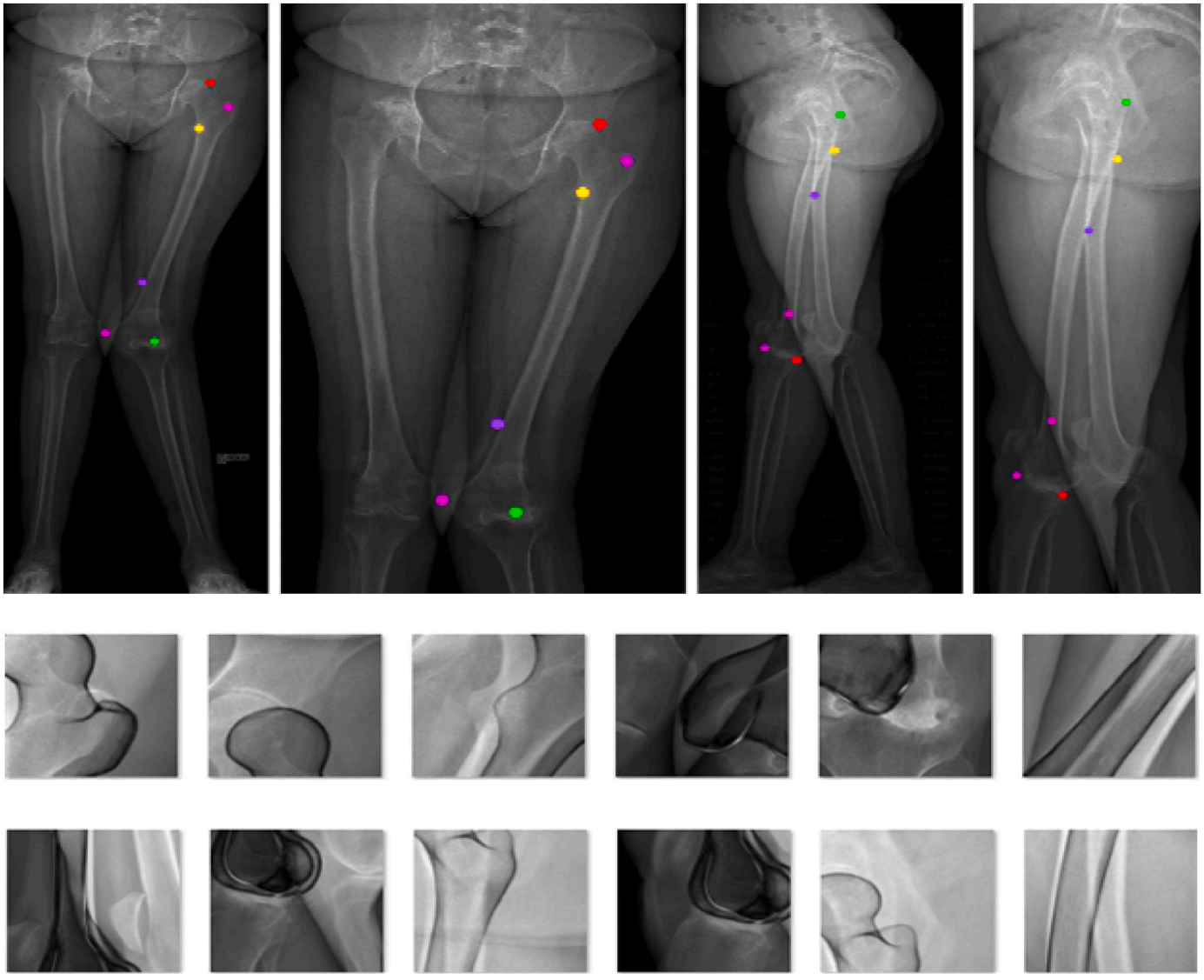

Fig. 4. First row: 2D projections of the six frontal (left) and lateral (right) pose-invariant 3D points on the left femur, after the coarse registration. Second and third row: six frontal and six lateral LIRs.Picture from Ref. [35].

Each CNN_i^{Shape} comprises two channels: the top channel deals with frontal local patches, while the bottom one covers lateral local patches (Fig. 3). This allows to directly estimate 3D displacements. The input and the structure of CNN_i^{Shape} are designed to obtain 3D displacements as output. The inverse of the 3D/2D similarity transformation, T^{-1}, is applied in the definition of the Euclidean loss function, as Eq. (7):

$$\psi = \frac{1}{n}\sum_{j=1}^{n}\left\| T_j^{-1}\left((\delta x,\delta y,\delta z)_j^{Target}\right) - T_j^{-1}\left((\delta x,\delta y,\delta z)_j\right)\right\|_2^2 \tag{7}$$

Where n is the number of samples and $T_j^{-1}\left((\delta x,\delta y,\delta z)_j^{Target}\right)$ and $T_j^{-1}((\delta x,\delta y,\delta z))$ are the known target and estimated 3D displacements for the j^{th} training sample, respectively.

3.4.1.2. Automatic 3D shape deformation. The automatic CNN-based computation of $\boldsymbol{CP}'$ allows to apply the MLS 3D shape deformation without any user annotations and interactions. Following the computation of new positions for the 17 3D handles, $\boldsymbol{CP}'$, to obtain an as-rigid-as-possible 3D shape deformation, the MLS method, described in Sec.3.1.1, is used to estimate regularized 3D displacements over all vertices of $\left(\boldsymbol{M}_g^{T}\right)$. The deformed model is called $\left(\boldsymbol{M}_g^{\hat{D}_s(T)}\right)$.

3.4.2. *Automatic 3D scale deformation* (U_{Scale})

Following $(CNNs^{Shape} + \text{MLS})$, to personalize the 3D scales of $\left(\boldsymbol{M}_g^{\hat{D}_s(T)}\right)$ according to the target bone $(\boldsymbol{F})$, we develop an automatic 3D scale deformation algorithm. (U_{Scale}) combines CNN-based regression models with a regularized MLS-based local 3D scale deformation to drive a fully automatic 3D scale deformation. The CNN-based regressors estimate local scale ratios corresponding to the 17 displaced handles, which are required to perform an as-rigid-as-possible MLS-based local 3D scale deformation without any user intervention.

3.4.2.1. CNN-based 3D scale ratios estimation. To adjust the scale of the 17 handles on $\left(\boldsymbol{M}_g^{\hat{D}_s(T)}\right)$, 17 CNN-based regressors are developed, with the same architecture as $\boldsymbol{CNNs^{Shape}}$, called $\boldsymbol{CNNs^{Scale}} = \left\{CNN_i^{Scale} | i = 1, \cdots, 17\right\}$, but with a different cost function, as Eq. (8):

$$\psi = \frac{1}{n}\sum_{j=1}^{n}\left\| (\delta s_x,\delta s_y,\delta s_z)_j^{Target} - (\delta s_x,\delta s_y,\delta s_z)_j\right\|_2^2 \tag{8}$$

Where n is the number of samples and $(\delta s_x,\delta s_y,\delta s_z)_j^{Target}$ and $(\delta s_x,\delta s_y,\delta s_z)_j$ are the known target and estimated scale ratio for the j^{th} training sample, respectively. The $\boldsymbol{CNNs^{Scale}}$ are independently trained to estimate the 3D scale ratios $\mathbf{SR}_{xyz} = \left\{(\delta s_x,\delta s_y,\delta s_z)_i \in \mathbb{R}^3 | i = 1,\ldots,17\right\}$ of the 17 displaced handles, $\boldsymbol{CP}'$. Among the set of 17 handles, $\boldsymbol{CP}'$, $\boldsymbol{cp}_1'$ to $\boldsymbol{cp}_{12}'$ are point handles with uniform scale $(s_x = s_y = s_z)_i$, and the corresponding regressors $\left\{CNN_i^{Scale} | i = 1,\cdots,12\right\}$ have one output in the last layer. $\boldsymbol{cp}_{13}'$ to $\boldsymbol{cp}_{17}'$, $\left(\left\{CNN_i^{Scale} | i = 13,\cdots,17\right\}\right)$ are the spline handles with non-uniform scale, which therefore have three outputs. Each CNN_i^{Scale} learns to regress a direct map function f_2 between the input 2D bi-planar (LIRs), Sec.3.2, and the output scale ratios, as Eq. (9):

$$f_2\left(LIRs\left(\boldsymbol{cp}_i', (DRR_F, DRR_L), (I_F, I_L)\right), \left(\boldsymbol{M}_g^{\hat{D}_s(T)}\right)\right)_i = (\delta s_x,\delta s_y,\delta s_z)_i \tag{9}$$

Where the input LIRs are local intensity differences, inside extracted local patches, between bi-planar digitally reconstructed radiographs (DRRs) of $\left(\boldsymbol{M}_g^{\hat{D}_s(T)}\right)$, as source (DRR_F, DRR_L), and patients' bi-planar radiographs as reference (I_F, I_L). The extracted local patches are centered at 2D projections of the 17 displaced handles, $\boldsymbol{CP}'$, on both frontal and lateral projections, at a size of 200 × 200 pixels.

3.4.2.2. Automatic 3D scaling. Following a CNN-based 3D scale ratios estimation, we automatically apply scaling over all vertices to personalize the scales of $\left(\boldsymbol{M}_g^{\hat{D}_s(T)}\right)$. The sum of weighted CNN-based local 3D scale ratios of the 17 handles over the sum of the computed weights, w_i, is computed to obtain the average of scale ratios over all handles, $\overline{SC}_{Local}$, Eq. (10). Then, the average of SC_{Global}, described in Sec. 3.1.1 (Eqs. (2) and (3)) , and $\overline{SC}_{Local}$, are calculated to obtain an optimal local scale $\widehat{SC}_{V_i}$, Eq. (11), as [10]:

$$\overline{SC}_{Local} = \frac{\boldsymbol{w}\cdot(\delta s_x,\delta s_y,\delta s_z)}{\sum_i w_i}.\ i = 1,\cdots,17 \tag{10}$$

$$\widehat{SC}_{\boldsymbol{v}_i} = \frac{(SC_{Global} + \overline{SC}_{Local})}{2} \tag{11}$$

Ultimately, each vertex $\boldsymbol{v}_i \in \left(V_g^{\hat{D}_s(T)}\right)$ is transformed with the computed optimal scale $\widehat{SC}_{\boldsymbol{v}_i}$ to extrapolate 3D scale deformation over $\left(\boldsymbol{M}_g^{\hat{D}_s(T)}\right)$ and obtain a personalized (deformed and rescaled) 3D bone model as $\left(\boldsymbol{M}_g^{\hat{S}_s(\hat{D}_s(T))}\right)$.

4. Data

4.1. 2D Bi-planar radiographs

After ethical approvals by the ethics committees of the University of Montreal Hospital Center (CHUM) and École de Technologie Supérieure (ÉTS, Montréal, Canada), a set of 2D bi-planar radiographs of 85 patients are retrospectively recovered. The whole femur is visible in the images. The set of 2D bi-planar radiograph are acquired from various fields of view, including the whole lower limbs and the full body, with two different patient orientations, 0°/90° and 45°/45°, by the low dose and slot-scanning EOS® system (EOS Imaging, Paris, France). We use a total of 70 patients, 56 for training and 14 for validation, in the training process. For testing, the remaining 15 unseen patients are then used.

4.2. Digitally reconstructed radiographs (DRRs)

The 2D bi-planar DRRs are rendered from the transformed and then deformed 3D model of the left femur $\left(\boldsymbol{M}_g^{\hat{D}_s(T)}\right)$, presented in Sec.3.4, using the Ray Casting method [44] via a home-made algorithm developed in C++, and running on an Intel® Core CPU. We render 85 bi-planar DRRs of $\left(\boldsymbol{M}_g^{\hat{D}_s(T)}\right)$, corresponding to 85 patients (training, validation, and test set).

4.3. Fuzzy gold standard personalized 3D models

To evaluate the performance of the 3D/2D registration, we compare the accuracy of the personalized 3D shape, 3D positions, and local scales of 17 handles with personalized fuzzy gold standard 3D models [43]. An expert constructed personalized fuzzy gold standard 3D models of the left femur, $(\boldsymbol{M}_{FGS})$, corresponding to 85 patients, using the semi-automatic commercial software, SterEOS [10,19], as an state-of-the-art (SOTA) method. For each patient, the set of 17 fuzzy gold standard handles, $\boldsymbol{CP}^{FGS}$, the corresponding 3D positions, and local scales are extracted from $(\boldsymbol{M}_{FGS})$. For each patient, the shape accuracy of the personalized 3D femur, 3D positions, and local scale of the 17 handles are compared with the corresponding personalized fuzzy gold standard 3D model and handles.

4.4. Gold standard CT-scan-based personalized 3D models

To evaluate the accuracy of the 3D reconstructed models by the proposed 3D/2D registration method, gold standard personalized 3D models are used as ground truths. The acquired CT 3D images and the corresponding CT-scan-based reconstructed 3D models of the left femur from five unseen pathological patients, who are different from the set of 85 patients, are used as gold standard personalized 3D models, ($\boldsymbol{M}_{GS}$). CT-scan-based personalized 3D models are reconstructed from CT-scan slices with manual segmentations by an expert via the SliceOmatic© software (Laporte et al., 2013). We have the EOS® 2D bi-planar radiographs of these five patients.

4.5. Training data for regression models

For each CNN_i^{Shape}, corresponding to each handle $\boldsymbol{cp}_i^T$, we extract 140 bi-planar LIs (Fig. 5) from a total of 70 patients' bi-planar radiographs. For all $CNNs^{Shape}$, corresponding to the set of 17 3D handles, we end up with (17 × 140) bi-planar LIs. To train $CNNs^{Scale}$ regression models, the same 70 patients' 2D bi-planar radiographs are considered as reference images. To train each CNN_i^{Scale} corresponding to $\boldsymbol{cp}_i^{'}$, 140 bi-planar LIRs (Fig. 6) of 70 patients are computed, leading to (17 × 140) bi-planar LIRs for the set of 17 $\boldsymbol{CP}^{FGS}$ to train 17 $CNNs^{Scale}$ models. In the second stage of the developed workflow, which is 3D shape and 3D scale deformation, we generated synthetic images for training CNNs. We used the same data augmentation technique that we applied in the first stage, 3D pose estimation [35]. For each patient, we generated 10 random perturbations around the 17 handles' fuzzy gold standard 3D displacements and 3D scale ratios. The perturbations follow a zero mean uniform distribution over the range of ±10 mm for 3D displacements in x, y and Z axis, and ±0.5 (%) for scale ratio. For 70 patients, we end up with 700 random 3D positions and scales for each 3D handle, leading to (17 × 1400) bi-planar LIs to train $CNNs^{Shape}$ regression models and (17 × 1400) bi-planar LIRs to train $CNNs^{Scale}$ models.

5. Experimental setup

5.1. 3D positions and 3D scale ratios of handles

5.1.1. Evaluation data and implementation

To evaluate the accuracy of the 3D position and local scale of the 17 handles of the personalized left femur, a set of 15 unseen patients' 2D bi-planar radiographs are used. From this set, nine and six bi-planar radiographs are acquired with 0°/90° and 45°/45° patients' orientations in the EOS® cabin system, respectively. We apply the two stages of the proposed 3D/2D registration workflow. The proposed method is implemented in a home-made software application and run on a GeForce® GTX GPU. For (U_{Shape}) and (U_{Scale}), the CNN-based regression models are developed in a Tensor-flow platform and implemented on a GeForce® GTX 1060 GPU. In each training iteration (epoch = 100), the mini-batch size is equal to 10, and the learning rate is 0.009. The weights are initialized using the Xavier method [38] and are learned using an Adam optimizer [39].

5.1.2. Evaluation metrics for 3D positions of handles

To evaluate the accuracy of the 3D positions of 17 handles, we compute the mean and standard deviation (Mean ±STD), the maximum (Max), and minimum (Min) of the absolute 3D Euclidean distance error (mm) between 3D positions of the 17 3D handles, $\boldsymbol{CP}^{'}$, computed by the proposed method, and the corresponding 17 fuzzy gold standard 3D positions, $\boldsymbol{CP}^{FGS}$, over 15 evaluation cases.

5.1.3. Evaluation metrics for 3D scale ratios of handles

To evaluate the accuracy of the local scale ratios of the 17 handles, we compute the mean and standard deviation (Mean ±STD), the maximum (Max), and minimum (Min) of the absolute scale ratio errors between the estimated $(\delta s_x, \delta s_y, \delta s_z)$ and the fuzzy gold standard scale ratios, $(\delta s_x, \delta s_y, \delta s_z)^{FGS}$, for the 17 handles over 15 evaluation cases. Of the 17 handles $\boldsymbol{CP}^{'}$, $\boldsymbol{cp}_1^{'}$ to $\boldsymbol{cp}_{12}^{'}$ are the point handles with uniform scale $(s_x = s_y = s_z)_i$, and the other five are the spline handles with non-uniform scale.

5.2. Personalized 3D femur and clinical measurement

5.2.1. Evaluation data and implementation

To evaluate the proposed fully automatic cascade-based CNN 3D/2D registration in the personalized 3D femur reconstruction and clinical 3D measurements application, the shape accuracy of the personalized 3D shape reconstruction of the left femur and the clinical 3D measurements are evaluated. We compare the accuracy of $\left(\boldsymbol{M}_g^{\hat{S}*(\hat{D}*(T))}\right)$ with two different evaluation sets: 1) fuzzy gold standard (M_{FGS}) of the 15 unseen patients described in Sec.4.3, and 2) ground truth gold standard (CT)-scan-based reconstructed 3D shape femurs ($\boldsymbol{M}_{GS}$) of a new set of five unseen patients, described in Sec.4.4.

5.2.1.1. First evaluation with fuzzy gold standard 3D models. The first evaluation compares our proposed fully automatic method with a semi-automatic approach [10] integrated in a commercial tool, SterEOS [10, 19], which is used to generate ($\boldsymbol{M}_{FGS}$) of the same 15 unseen patients. The main objective of the first evaluation is to validate the effectiveness and potential of the proposed automatic method to be integrated in the clinical practice by looking at how our results are close to those obtained by the semi-automatic commercial SterEOS tool [10,19]. This evaluation compares the shape accuracy of the 3D personalized femur and clinical measurements obtained by the proposed automatic method and the results of the current clinical tool [10,19]. Importantly, the generic 3D model, that we deform to obtain the personalize 3D femur, has been previously validated [10,19] to be used in clinical practice and the extracted clinical parameters are within the acceptable accuracy.

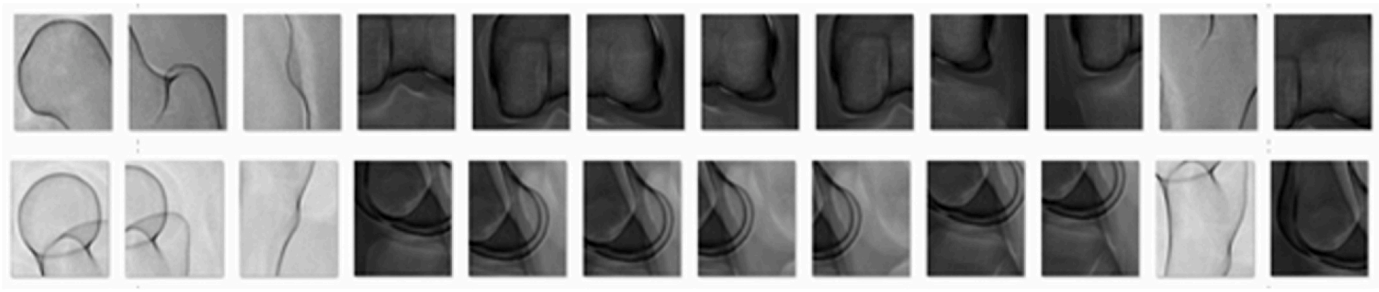

Fig. 5. Illustration of 12 frontal LIRs (top) and lateral LIRs (bottom) centered at 2D projection of 3D handles with uniform scaling *CP*′to *CP*.

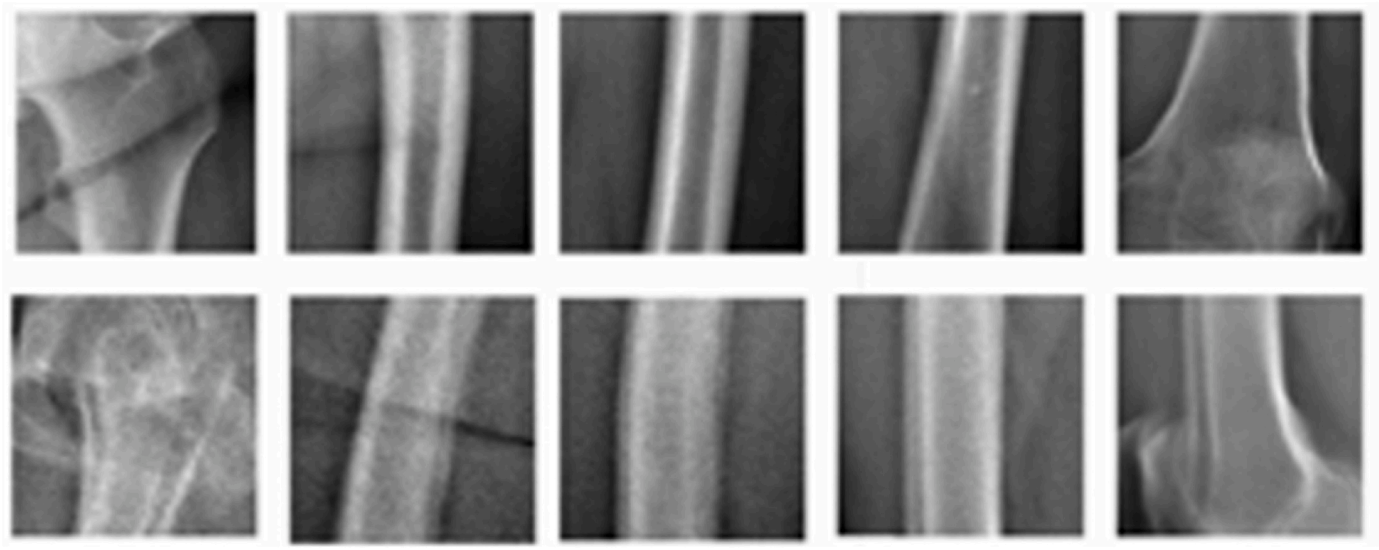

Fig. 6. Illustration of 12 frontal LIRs (top row) and lateral LIRs (bottom row) centered at 2D projections of 5 3D handles with non-uniform scaling CP' to CP'.

5.2.1.2. Second evaluation with gold standard CT-scan-based 3D model reconstruction. In the second evaluation, the shape accuracy of the personalized 3D femur $\left(\boldsymbol{M}_g^{\hat{S}_o(\hat{D}_o(T))}\right)$ is compared with the corresponding gold standard CT-scan-based model $(\boldsymbol{M}_{GS})$. We firstly apply the Iterative Closest Point (ICP) rigid registration method [40] to align the estimated $\left(\boldsymbol{M}_g^{\hat{S}_o(\hat{D}_o(T))}\right)$ into $(\boldsymbol{M}_{GS})$, for transfer into the same 3D coordinate system. Then, the shape accuracy (Section 5.2.2) is computed between $\left(\boldsymbol{M}_g^{\hat{S}_o(\hat{D}_o(T))}\right)$ and $(\boldsymbol{M}_{GS})$.

5.2.1.3. Evaluation of clinical measurement. In addition to the accuracy of the computation of the personalized 3D shape reconstructed femur, four important clinical 3D measurements of the personalized 3D shape of femurs are computed via a commercial tool integrated in SterEOS software [10]. These extracted 3D measurements are: 1) hip knee center-femoral shaft angle (HKS), which is the angle between the mechanical and anatomical femoral axis, 2) femoral mechanical angle (FMA), 3) femoral torsion (FT), which is the angle between the femoral neck axis and the bicondylar femoral axis, and 4) femoral length (FL).

5.2.2. Evaluation metrics

The shape accuracy of the reconstructed personalized 3D model of the left femurs is evaluated based on two different measurements, namely, the point-to-surface (P2S) distance and the 3D Hausdorff distance errors. We compute the Root Mean Square (RMS), Mean, Min, and Max of (P2S) distance errors (mm) between the estimated $\left(\boldsymbol{M}_g^{\hat{S}_o(\hat{D}_o(T))}\right)$ and the corresponding $(\boldsymbol{M}_{FGS})$ and $(\boldsymbol{M}_{GS})$. To evaluate the clinical 3D measurements, we compute the Mean and Standard Deviation of Absolute Errors (MAE ±STD) of four clinical 3D measurements of the left femur, separately, between the estimated $\left(\boldsymbol{M}_g^{\hat{S}_o(\hat{D}_o(T))}\right)$ and fuzzy gold standard $(\boldsymbol{M}_{FGS})$, in mm and degrees.

6. Results

6.1. 3D displacement accuracy of handles

Fig. 7 illustrates the quantitative results of the computed 3D position accuracy for the 17 handles. For each handle, the black dot, red line, top and bottom of blue line caps show (Mean ±STD), (Max), and (Min) errors, respectively.

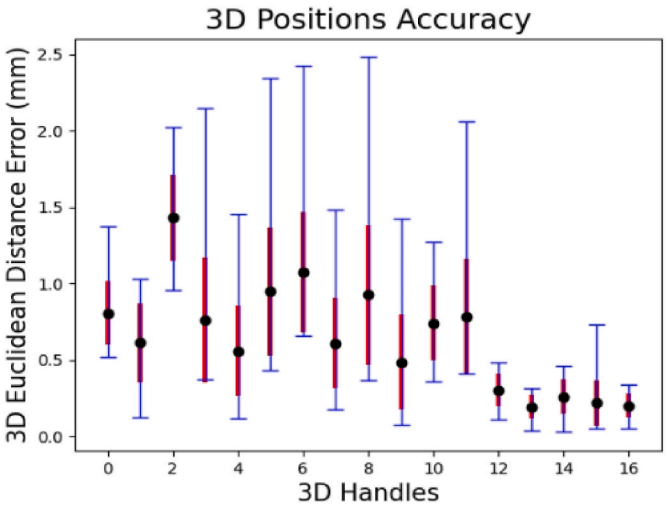

Fig. 7. Error bars of computed 3D positions of 17 handles.

6.2. 3D scale ratio accuracy of handles

Fig. 8 illustrates the quantitative results of the local 3D scale ratio accuracy for the 17 handles estimated by the CNN^{Scale} regression models. For each handle, the black dot, red line, top and bottom of blue line caps show the (Mean ±STD), (Max), and (Min) errors, respectively. In Fig. 8, for 5 non-isotropic handles, $\boldsymbol{cp}'_{13}$ to $\boldsymbol{cp}'_{17}$, we show the maximum scale errors for the X-, Y-, and Z-axes.

6.3. Personalized 3D femur accuracy

Table 1 presents the average of (RMS, Mean, STD, Min, Max) of point-to-surface (P2S) distance errors (mm) between the personalized 3D femurs $\left(\boldsymbol{M}_g^{\hat{S}_o(\hat{D}_o(T))}\right)$ and the corresponding fuzzy gold standards $(\boldsymbol{M}_{FGS})$ over 15 evaluation cases. The (Mean ±STD) of the 3D Hausdorff distance errors over 15 unseen patients is equal to 2.95 ± 1.42 mm. Table 2 depicts the mean and standard deviation of absolute errors of four clinical 3D measurements extracted from personalized 3D femurs in comparison with the corresponding fuzzy gold standard models of 15 unseen patients.

Fig. 9 presents RMS-P2S errors of personalized 3D femur of 15

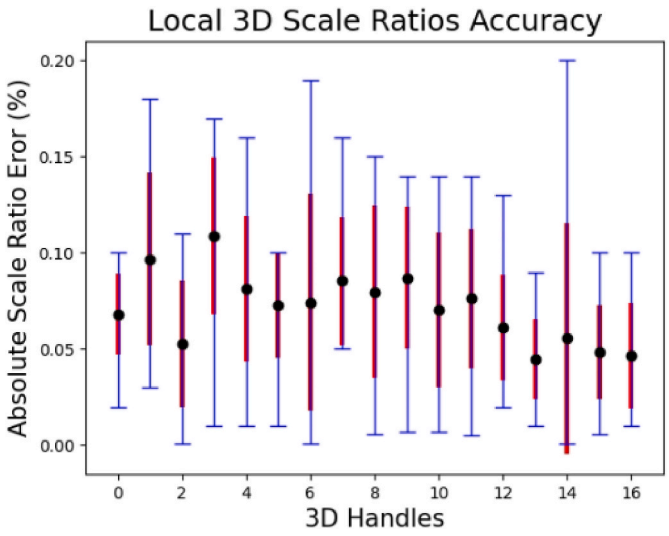

Fig. 8. Error bars of local 3D scale ratios of 17 handles.

Table 1
Average (Ave.) of (RMS, Mean, STD, Min, Max) of P2S distance errors (mm) in comparison with fuzzy gold standard 3D models.

Error	RMS	Mean	STD	Min	Max
Ave.	0.88	0.66	0.57	9.77E-05	2.87

Table 2
(MAE ±STD) of four clinical measurements in degrees (°) and (mm) over 15 reconstructed 3D femurs in comparison with fuzzy gold standard 3D models.

Error	HKS (°)	FMA (°)	FT(°)	FL (mm)
Mean	0.14	0.09	0.16	0.67
STD	0.09	0.09	0.12	0.35

patients in comparison with fuzzy gold standard 3D models. Table 3 for its part presents and compares the accuracy of the personalized 3D femurs $\left(\boldsymbol{M}_g^{\hat{S}_s(\hat{D}_s(T))}\right)$ via the proposed methodology and semi-automatic commercial SterEOS tools [10] in comparison with the ground truth gold standard 3D models ($\boldsymbol{M}_{GS}$), for the same five patients. The average of (RMS, Mean, STD, Min, Max) of point-to-surface (P2S) distance errors (mm) are computed over five unseen patients.

Fig. 10 shows P2S distance map between a personalized 3D femur via the proposed method and the corresponding fuzzy gold standard model, reconstructed by the semi-automatic commercial SterEOS software [10], for one of the validation cases. Fig. 11 shows P2S distance map between a personalized 3D femur via the proposed method and the corresponding CT-scan-based gold standard 3D model for one of the validation cases.

7. Discussion

The proposed fully automatic CNN cascade-based 3D/2D registration framework combines an automatic coarse-to-fine CNN-based 3D/2D similarity registration and an automatic CNN-based 3D/2D non-rigid registration. The goal is to have a personalized 3D femur reconstruction and clinical 3D measurements from 2D bi-planar EOS® radiographs. The main benefit of this work leads clinicians to easily adopt and use this method, as it in fact contributes to an existing and established software tool. In 3D/2D non-rigid registration, CNN cascade-based regression models are successfully merged with MLS 3D shape and scale deformation (Table 1). Unlike a semi-automatic MLS deformation integrated in SterEOS [10], which needs user interventions to annotate the new positions of 17 3D controls and to manually adjust the scales, the proposed CNN-based regressors provide significant advantages for: 1) removing operator interventions, and 2) fast adjustments of 3D handles' positions and scales, to drive MLS 3D shape and scale deformation (Fig. 7). In comparison with fuzzy gold standard 3D handle positions, the average of the Mean Absolute Errors (MAE) of 3D Euclidean distance of the 17 3D handles' positions on 15 validation cases is equal to 0.63 mm. Using CNN allows us to achieve a Mean of 3D Euclidean distance errors lower than 1 mm for each of the 15 3D handles, except for C3 (1.42 mm) and C7 (1.07 mm) (Fig. 7). C3 and C7 correspond to the smaller trochanter and the posterior exterior condyle, respectively, which are less visible than other 3D handles due to the overlap between the bone structures, mostly in patients with a 0°/90° orientation. Unlike [9], which uses FFD deformation on a large set of 3D control points (88), using the MLS deformation on a small set of 17 handles allows clinicians to easily correct potential reconstruction errors [9]. uses the triangulation-based method to compute the corresponding 3D positions of updated 2D bi-planar positions of the projected 3D control points; this is done by direct estimation of the 3D displacements at the origin $(0, 0, 0)$ of the 3D referential of the EOS® cabin system. By contrast, our contribution to a 3D/2D non-rigid registration involves fewer steps.

The developed 17 CNN-based local 3D scale ratio regressors auto-

Table 3
Average (Ave.) of (RMS, Mean, STD, Min, Max) of P2S distance errors (mm) as compared to CT-scan-based gold standard 3D models.

	Error	RMS	Mean	STD	Min	Max
Proposed method	Ave.	2.70	2.14	1.64	0	11.08
Semi-automatic SterEOS tool [10]	Ave.	2.07	1.47	1.19	6.8E-04	10.07

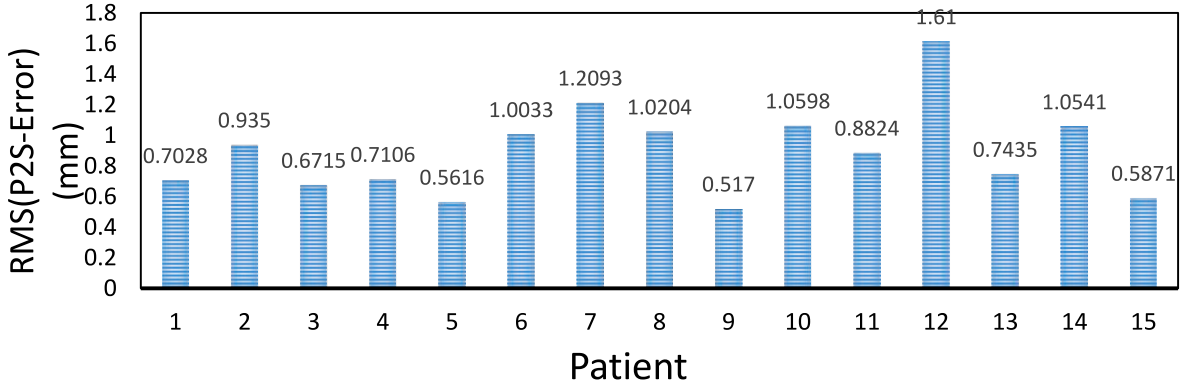

Fig. 9. Illustration of RMS-P2S error of reconstructed personalized 3D femurs for 15 patients in comparison with fuzzy gold standard 3D models. (For interpretation of the references to colour in this figure legend, the reader is referred to the Web version of this article.)

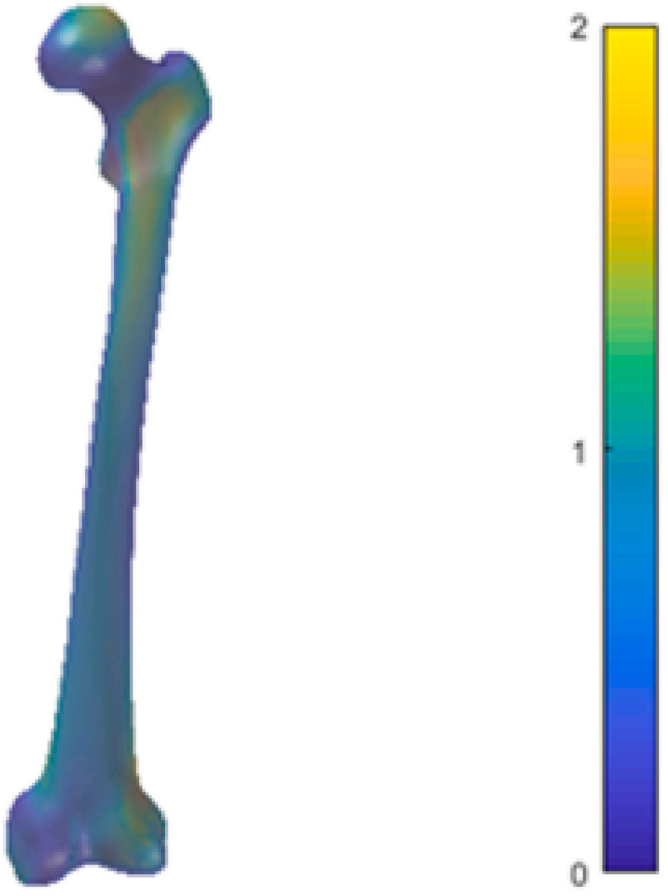

Fig. 10. Distance map of the P2S error on a personalized 3D femur of a patient with a 0°/90° orientation in comparison with fuzzy gold standard model (left) and error bar (right) showing minimum (0) and maximum (2) error in (mm). (For interpretation of the references to colour in this figure legend, the reader is referred to the Web version of this article.)

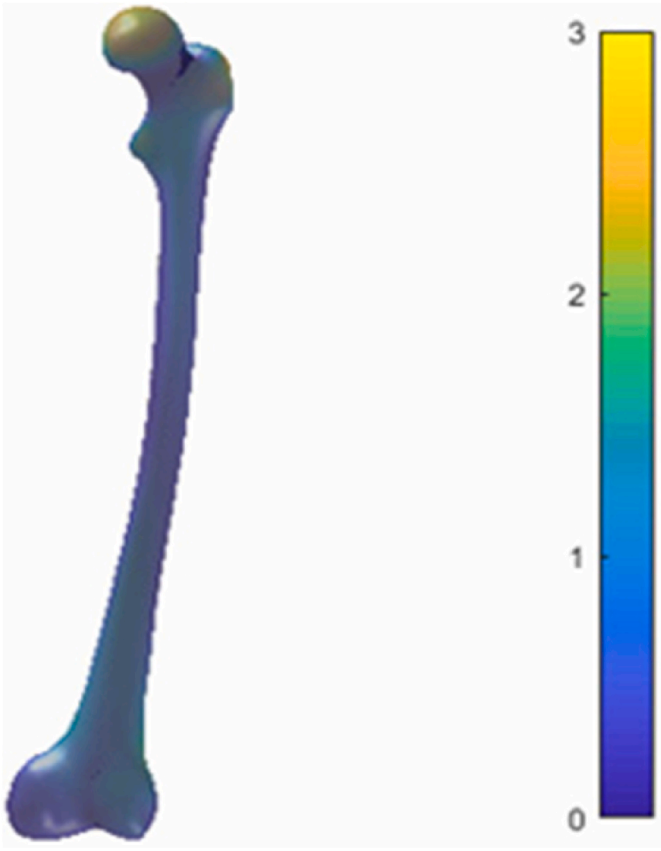

Fig. 11. Distance map of the P2S error on a personalized 3D femur of a patient with a 45°/45° orientation in comparison with CT-scan-based gold standard model (left) and error bar (right) showing minimum (0) and maximum (3) error in (mm). (For interpretation of the references to colour in this figure legend, the reader is referred to the Web version of this article.)

matically provide personalized local scale ratios corresponding to the 17 3D handles. Merging CNN-based local 3D scale ratio regressors with MLS deformation automatically adjusts the 2D silhouette of the 3D femur with the edges of the target bone in patients' 2D bi-planar radiographs. Compared to fuzzy gold standard 3D handle scale ratios, using CNN to estimate the local scale ratios of 17 3D handles provides an MAE lower than 0.1 % over 15 validation cases for each handle (Fig. 8). The mean of the MAE of the 17 3D handles is equal to 0.05 %. C15 (spline diaphysis with non-uniform scale) and C7 (condyle posterior exterior with uniform scale) are two 3D handles that have Min $\left(Es_x = 0.05\%, Es_y = 0.03\%, Es_z = 0.05\%\right)$ and Max (0.1 %) of MAE, respectively.

The computation time for the 3D femur reconstruction via the proposed fully automatic 3D/2D registration framework, without any code optimization, is 75 s, using a GeForce® GTX 1060 GPU and an Intel® Core I7 CPU. Hence, using automatic CNN-based 3D pose initialization and CNN-based 3D/2D registration improves the computation time as compared to Ref. [10], which is a semi-automatic method and requires 10 min for the reconstruction of both lower limbs with CPU computation. Regarding hardware adaptability, since the proposed method automates MLS-based 3D femur reconstruction method [10], integrated in the existing and established semi-automatic commercial SterEOS software tool [19], with the ability to easily adapt to different hardware environment including GPU and CPU-based systems in clinical routines, hence our proposed method has ability to be easily adapted into different hardware environment making it suitable for the clinical routine setting. In comparison with other relevant works, in Ref. [18], a conventional iterative optimization is used to reconstruct a personalized 3D proximal femur, with a reported time of 15 min, with CPU computation. However, in Ref. [24], the computation time of [18] is improved to 1.09 s with GPU computation.

The personalized 3D femur shape accuracy is validated in comparison with two different validation sets. In the first validation, we compare the shape accuracy of the personalized 3D femurs with fuzzy gold standard 3D models reconstructed via the semi-automatic approach integrated in the commercial software, SterEOS [10,19]. The (Mean ± STD) of RMS-P2S errors over 15 validation cases is equal to 0.88 ± 0.29 mm (Table 1). The Mean of Max-P2S errors is 2.87 mm (Table 1) [10]. presents a Mean of 1.0 mm and Max of 6.6 mm in comparison to CT-scan, and [19–22] show that this semi-automatic method [10] has significant accuracy for lower limbs deformation diagnosis and it is a very useful tool in the current clinical routines. Therefore, the results of our automatic method are close to those obtained by Ref. [10] and, with the current accuracy, it has a strong potential to be used as a practical diagnostic tool and be implemented in clinical routines.

After 3D femur reconstruction, four clinical measurement errors are computed in comparison with the semi-automatic software SterEOS tools [10,19], on the same validation set. The MAE and STD of each clinical 3D measurement are lower than 1 mm or 1° (Table 2) and are very close to those obtained by Ref. [10,19–22] demonstrate that [10] is a very useful tool to assist physicians to measure lower limbs clinical parameters, so our automatic method also can be used to measure clinical parameters. In the clinical routine of 3D model-based orthopedic applications, the proposed automatic and fast CNN cascade-based

3D/2D registration achieves a high accuracy for clinical 3D measurement computation to help clinicians quickly diagnose and analyze 3D shape deformities in the femur. For the first validation set, a 100 % success rate is achieved for RMS-P2S errors lower than 1 mm for the reconstructed personalized 3D femurs (Table 1).

For the second validation set, the (Mean ±STD) of RMS-P2S errors of five personalized 3D femurs in comparison with CT-scan-based gold standard 3D models is equal to 2.70 ± 0.39 (Table 3, first row). The Mean of Max-P2S error is 11.08 mm (Table 3, first row). The second row of Table 3 presents the accuracy of the semi-automatic commercial software SterEOS [10], which is already integrated in the existing clinical routine, in comparison to the ground truth CT-based 3D models for the same five patients. Table 3 shows that the proposed automatic method presents similar results to the semi-automatic method established in the commercial SterEOS tool [10]. Our results are like those obtained by Ref. [10] which physicians are currently using in the clinical routines [19–22]. Hence the proposed automatic framework with the current accuracy has the power of the practical usability for lower limbs deformation diagnosis in the clinical routines. The differences between the two evaluation results (Tables 1 and 3, first row) arise from the fact that, in the first validation set, the fuzzy gold standard models are the reconstructed 3D models from the same generic 3D femur with the same 17 handles that are used in the proposed methodology. On the other hand, in the second validation set, gold standards are CT-scan-based 3D models reconstructed by manual segmentations of the femur boundaries on CT slices. The CT-scan-based gold standard 3D models are more accurate than the fuzzy gold standard 3D models, so the 3D reconstruction errors of the second validation set are larger than in the first validation set. Fig. 10 shows the distance P2S error map with RMS-P2S of 0.5 mm between a personalized 3D femur and fuzzy gold standard model of a patient with a 0°/90° orientation. Fig. 11 depicts the distance P2S error map with RMS-P2S of 1.03 mm between a personalized 3D femur and CT-scan-based gold standard 3D model of a patient with a 45°/ 45° orientation. The second validation, which uses gold standard 3D models constructed from CT-scans via manual segmentation, serve to validate that the proposed approach, even if it is not able to exactly reproduce every small detail on the surface of the bones because of the limited degrees of freedom of the underlying 3D generic model, is still a very good representation of the shape of the bone, as shown in Table 3. The reconstructed 3D model is flexible enough to still represent the shape of the femur with good accuracy.

In comparison to Voxel Morph [32], which is a deep-learning based non-rigid registration between 3D MRI volume and an atlas without any landmarks, we developed a personalized approach to fit a generic 3D femur into patient's 2D radiographs to construct the patient-specific 3D femur model to quantify 3D clinical measurements which are essential for clinicians in preoperative planning. For an intensity-based non-rigid registration, VoxelMorph iteratively combines CNN, to estimate registration field, and a linear interpolation-based spatial transformation, to warp the source 3D image into an atlas. In our method, to automate MLS deformation, we train 17 CNNs to estimate 3D displacement fields and 3D scale ratios of 17 handles, which are required as input for MLS deformation. Then, the MLS method starts to deform the 3D femur to fit into patient's 2D radiographs. In contrast to the VoxelMorph, which does not use any landmarks for non-rigid registration, in our method the 3D position and scale of the 17 handles, which are essential to measure 3D geometric parameters of the femur, in clinical routines. The MLS deformation [10], provides clinicians with a user-friendly way to easily adjust, if required, the reconstructed 3D model via a small number of MLS handles. However, VoxelMorph, used large number of voxels for spatial transformation, which makes impossible the adjustment of the errors after non-rigid registration. The main advantage of our method is its ease of adoption by clinicians and seamlessly integrating with existing commercial SterEOS software [19] by automatically estimating 3D handles. The VoxelMorph reported the Dice score metric as nonrigid registration, however, we reported P2S distance error of the reconstructed 3D model after non-rigid registration. VoxelMorph reports the runtime of less than 1 s for non-rigid registration via GPU, without considering affine transformation of the preprocessing step. In our method, all stages of 3D/2D registration framework takes 75 s, using both GPU and CPU computations.

Notwithstanding difficulties in comparing the accuracy of different methods validated based on non-similar databases, experiments, evaluation metrics, and applications, we compare the accuracy of the personalized 3D femurs with the most relevant state-of-the art results in 3D model-based orthopedic applications. In contrast to Ref. [25], a semi-automatic 3D femur reconstruction with a manual 3D pose initialization, which optimizes MLS handles of the generic 3D femur via a conventional iterative method, CNN cascade-based regression models are trained to optimize the MLS handles of the generic 3D femur. In Ref. [25], the average of the Mean-P2S distance errors on six femurs is 1.0 mm, and the Max of Mean-P2S is 5.53 mm. In contrast to conventional iterative optimization methods in semi-automatic 3D/2D non-rigid SSM registration [8,11,16,18,24], we develop CNN cascade-based regression models for a fast and automatic 3D/2D non-rigid registration of the generic 3D model of the femur in patients' 2D bi-planar EOS® radiographs. In the proposed fully automatic 3D/2D registration, we reach an average RMS-P2S distance error of 2.70 mm for the whole femur reconstruction [8,16]. report an average RMS-P2S distance error of 1.68 mm and 1.48 mm, respectively, in a semi-automatic 3D/2D registration for personalized 3D distal femur reconstruction with manual pose initialization. In (Yu et a., 2015; [9]), the mean accuracy of personalized 3D proximal femur reconstruction is equal to 1.5 mm and 1.3 mm in a semi-automatic and automatic intensity-based 3D/2D non-rigid registration, respectively. However [18], requires a manual 3D pose initialization. In Ref. [9], the proposed automatic 3D/2D registration uses FFD deformation with a large set of control points. This approach requires a strong regularization to avoid undesirable distortions in 3D bone reconstruction. Moreover, after the 3D reconstruction process, if a manual adjustment were needed to correct 3D model errors, it would be difficult for clinicians to manually adjust a large set of control points. In contrast, using the MLS deformation, which is deployed as part of the commercial SterEOS software tools [10,19], provides an as-rigid-as-possible shape deformation without undesirable distortion on a small set of 3D handles. Moreover, the proposed automatic CNN cascade-based 3D/2D registration merged with the MLS deformation is more appropriate for clinicians in clinical routine as they retain the capacity to quickly and easily adjust reconstructed 3D femur models.

As the limitation of our method, we can see the largest errors are located around trochanter and posterior exterior condyle which are less visible than other 3D handles due to the overlap between the bone structures. In further works, to speed up the 3D shape and local 3D scale deformation, we can estimate 3D displacement of the 17 handles in a parallel computation to speed up the performance. Afterward, we can estimate local 3D scaling of 17 handles in a parallel computation to speed up the performance. In addition, to generalize the proposed method, we will use different image sets from different hospitals to train CNN-based models. In this work, we used EOS 2D bi-planar radiographs which provide high quality images with patients. In the case of using different imaging systems with poor image qualities, to improve contrast, reduce noise, and enhance anatomical boundaries, we will use an appropriate image processing step to enhance image qualities prior training CNN-based regression models [41,42]. The proposed approach utilizes 2D bi-planar images of equal resolution, rotated 90° relative to one another, for the 2D/3D registration process. This setup aligns with the output format of the EOS system, which generates a pair of X-ray images with similar imaging characteristics and spatial calibration relative to the cabin reference frame. This is not considered a limitation, as the method is specifically designed to operate on EOS-generated images. Importantly, aside from the requirement that input images are acquired using the EOS system, there is no other limitation with respect

to the size or the resolution. The proposed approach will certainly work for images produced by different devices, even if the resolutions of the devices are different. This is the case because the 3D model is registered to the images in a two-stages approach in which the first approximation is obtained by a similarity transformation including a scale parameter. During CNNs training, we added a data augmentation strategy to generate input image patches at different scales, which effectively makes the 3D/2D registration process invariant to size and resolution variations. This generalizability is supported and clearly demonstrated in the quantitative results presented in Table 1, which includes individuals of different sizes.

8. Conclusion

The presented fully automatic CNN cascade-based 3D/2D non-rigid registration framework efficiently registers the generic 3D model of the femur into 2D bi-planar EOS® radiographs to assess clinical 3D geometrical parameters. The proposed CNN-based 3D handles displacement and scale ratio estimation eliminates manual annotations and user interventions for MLS deformation and does so in a time-efficient manner. In clinical 3D geometrical parameter assessment of the femur, this method provides physicians with the capacity to easily adjust possible errors of the reconstructed 3D model. We achieve an average RMS-P2S accuracy of 0.88 and 2.70 mm in evaluations with respect to a fuzzy gold standard and CT-scan-based ground truth gold standard 3D models, respectively. Four clinical 3D measurements of the reconstructed 3D femurs are evaluated in comparison with the fuzzy gold standard 3D models. The MAE of each clinical 3D measurement is lower than 1 mm or 1°. When compared to the previous semi-automatic method [10,19], the results obtained with the proposed automatic system are promising, and the system can be used efficiently for other lower limbs bone structures, such as the tibia. The context of the 3D femur model reconstruction is rich with potential applications and development of the prototypes opens the door to possible research opportunities. Following the accomplishment of this project, as future work, we will apply the proposed system on 3D pose estimation of the knee flexion, since we trained CNN-based 3D pose estimation models with generated DRRs of the femur with the knee flexions until 15°. It will need some modification on the model's development and then validation of the model, since the structure of the knee bone differs from the femur and we developed this 3D pose estimation model for the femur bone.

CRediT authorship contribution statement

Nahid Babazadeh Khameneh: Writing – review & editing, Writing – original draft, Visualization, Validation, Software, Methodology, Formal analysis, Conceptualization. **Thierry Cresson:** Writing – review & editing, Resources, Methodology, Conceptualization. **Frédéric Lavoie:** Writing – review & editing, Resources, Funding acquisition. **Jacques de Guise:** Resources, Project administration, Funding acquisition, Conceptualization, Writing – review & editing, Supervision. **Carlos Vázquez:** Writing – review & editing, Supervision, Resources, Project administration, Methodology, Funding acquisition, Conceptualization.

Ethics statement

We confirm that for this study, after ethical approvals by the ethics committees of the University of Montreal Hospital Center (CHUM) and École de Technologie Supérieure (ÉTS, Montréal, Canada), a set of 2D bi-planar radiographs of 85 patients were retrospectively recovered.

Declaration of competing interest

The authors declare the following financial interests/personal relationships which may be considered as potential competing interests: Nahid Babazadeh Khameneh reports was provided by Natural Science and Engineering Research Council of Canada (NSERC). Nahid Babazadeh Khameneh reports financial support was provided by Quebec Consortium for Industrial Research and Innovation in Medical Technology, Canada, (MEDTEQ). Nahid Babazadeh Khameneh reports financial support was provided by Mathematics of Information Technology and Complex Systems, Canada, (MITACS). Nahid Babazadeh Khameneh reports financial support was provided by EOS Image Inc, Paris, France. If there are other authors, they declare that they have no known competing financial interests or personal relationships that could have appeared to influence the work reported in this paper.

Acknowledgments

The authors thank EOS Image Inc. and the LIO laboratory software team for constructing the reference 3D models. This work was supported by the Natural Science and Engineering Research Council of Canada (NSERC) [RDCPJ 518301]; the Quebec Consortium for Industrial Research and Innovation in Medical Technology, Canada, (MEDTEQ) [11-O]; the Mathematics of Information Technology and Complex Systems, Canada, (MITACS) [IT08573]; and the EOS Image Inc, Paris, France.

References

[1] B. Cretuet, Z. Panti, M. Nica, B. Serban, M. Popa, R. Ene, C. Cirstoiu, Lower limb deformity and total knee replacement, Rom. J. Orthop. Surg. Traumatol. 1 (2) (2019) 121–127, https://doi.org/10.2478/rojost-2018-0090.
[2] S.V. Drongelen, H. Kaldowski, B. Fey, T. Tarhan, A. Assi, F. Stief, A. Meurer, Determination of leg alignment in hip osteoarthritis patients with the EOS® system and the effect on external joint moments during gait, Appl. Sci. 10 (21) (2020) 1–14, https://doi.org/10.3390/app10217777.
[3] S. Hosseinian, H. Arefi, 3D reconstruction from multi-view medical X-ray images - review and evaluation of existing methods, Int. Arch. Photogram. Rem. Sens. Spatial Inf. Sci. 40 (1) (2015) 319–326, https://doi.org/10.5194/isprsarchives-XL-1-W5-319-2015.
[4] B. Goswami, S. Kr Misra, 3D modeling of X-Ray images: a review, Int. J. Comput. Appl. 132 (7) (2015) 40–46, https://doi.org/10.5120/ijca2015907566.
[5] C.J.F. Reyneke, M. Luthi, V. Burdin, T.S. Douglas, T. Vetter, T.E.M. Mutsvangwa, Review of 2-D/3-D reconstruction using statistical shape and intensity models and X-Ray image synthesis: toward a unified framework, IEEE Rev. Biomed. Eng. 12 (2019) 269–286, https://doi.org/10.1109/RBME.2018.2876450.
[6] P. Cerveri, A. Belfatto, A. Manzotti, Predicting knee joint instability using a tibio-femoral statistical shape model, Front. Bioeng. Biotechnol. 8 (2020) 1–12, https://doi.org/10.3389/fbioe.2020.00253.
[7] E.S. Abebe, G.M. Utturkar, D.C. Taylor, C.E. Spritzer, J.P. Kim, C.T. Moorman III, W.E. Garrett, Defrate, The effects of femoral graft placement on in vivo knee kinematics after anterior cruciate ligament reconstruction, J. Biomech. 44 (5) (2011) 924–929, https://doi.org/10.1016/j.jbiomech.2010.11.028.
[8] N. Baka, B.L. Kaptein, M. De Bruijne, T. van Walsum, J.E. Giphart, W.J. Niessen, B. P.F. Lelieveldt, 2D-3D shape reconstruction of the distal femur from stereo X-ray imaging using statistical shape models, Med. Image Anal. 5 (6) (2011) 840–850, https://doi.org/10.1016/j.media.2011.04.001.
[9] W. Yu, C. Chu, M. Tannast, G. Zheng, Fully automatic reconstruction of personalized 3D volumes of the proximal femur from 2D X-ray images, Int. J. Comput. Assist. Radiol. Surg. 11 (9) (2016) 1673–1685, https://doi.org/10.1007/s11548-016-1400-9.
[10] Y. Chaibi, T. Cresson, B. Aubert, J. Hausselle, P. Neyret, O. Hauger, Fast 3D reconstruction of the lower limb using a parametric model and statistical inferences and clinical measurements calculation from biplanar X-rays, Comput. Methods Biomech. Biomed. Eng. 15 (5) (2012) 457–466, https://doi.org/10.1080/10255842.2010.540758.
[11] K. Youn, M.S. Park, J. Lee, Iterative approach for 3D reconstruction of the femur from un-calibrated 2D radiographic images,", Med. Eng. Phys. 50 (2017) 89–95, https://doi.org/10.1016/j.medengphy.2017.08.016.
[12] M. Fleute, S. Lavallée, Nonrigid 3-D/2-D registration of images using statistical models, Med. Image Comput 1679 (1999) 138–147, https://doi.org/10.1007/10704282_15. Comput. Asssist. Interv. (MICCAI), Lect. Notes Comput. Sci.
[13] D. Mitton, C. Landry, S. Veron, W. Skalli, F. Lavaste, J.A. De Guise, 3D reconstruction method from biplanar radiography using non-stereocorresponding points and elastic deformable meshes, Med. Biol. Eng. Comput. 38 (2000) 133–139, https://doi.org/10.1007/BF02344767.
[14] S. Laporte, W. Skalli, J.A. De Guise, F. Lavaste, D. Mitton, A biplanar reconstruction method based on 2D and 3D contours: application to the distal femur, Comput. Methods Biomech. Biomed. Eng. 6 (1) (2003) 1–6, https://doi.org/10.1080/1025584031000065956.
[15] M.R. Mahfouz, A. Badawi, E.E. Abdel Fatah, M. Kuhu, B. Merkl, Reconstruction of 3D patient-specific bone models from biplanar X-ray images utilizing

morphometric measurements, in: Int. Conf. Image Process. Comput. Vision (IPCV, 2006, pp. 345–349.
[16] N. Baka, M. De Bruijne, T. Van Walsum, B.L. Kaptein, J.E. Giphart, M. Schaap, Statistical shape model-based femur kinematics from biplane fluoroscopy, IEEE Trans. Med. Imag. 31 (8) (2012) 1573–1583, https://doi.org/10.1109/TMI.2012.2195783.
[17] B. Aubert, C. Vazquez, T. Cresson, S. Parent, J.A. De Guise, Toward automated 3D spine reconstruction from biplanar radiographs using CNN for statistical spine model fitting, IEEE Trans. Med. Imag. 38 (12) (2019) 2796–2806, https://doi.org/10.1109/TMI.2019.2914400.
[18] W. Yu, P. Zysset, G. Zheng, Personalized x-ray reconstruction of the proximal femur via a non-rigid 2D-3D registration, Proc. SPIE Med. Imaging 9413 (2015), https://doi.org/10.1117/12.2082339.
[19] E. Melhem, A. Assi, R. El Rachkidi, I. Ghanem, EOS® biplanar X-ray imaging: concept, developements, benefits, and limitations, J. Child Orthop. 10 (1) (2016) 1–14, https://doi.org/10.1007/s11832-016-0713-0.
[20] A. Assi, Y. Chaibi, A. Presedo, J. Dubousset, I. Ghanem, W. Skalli, Three-dimensional reconstructions for asymptomatic and cerebral palsy children's lower limbs using a biplanar X-ray system: a feasibility study, Eur. J. Radiol. 82 (12) (2013) 2359–2364, https://doi.org/10.1016/j.ejrad.2013.07.006.
[21] D. Folinais, P. Thelen, C. Delin, C. Radier, Y. Catonne, J.Y. Lazennec, Measuring femoral and rotational alignment: EOS system versus computed tomogr aphy, Orthop. Traumatol.: Surg. Res. 99 (5) (2013) 509–516, https://doi.org/10.1016/j.otsr.2012.12.023.
[22] E. Gaumetou, S. Quijano, B. Ilharreborde, A. Presedo, P. Thoreux, K. Mazda, W. Skalli, EOS analysis of lower extremity segmental torsion in children and young adults, Orthop. Traumatol Surg. Res. 100 (1) (2014) 147–151, https://doi.org/10.1016/j.otsr.2013.09.010.
[23] L. Fang, Z. Wang, Z. Chen, F. Jian, S. Li, H. He, 3D shape reconstruction of lumbar vertebra from two X-ray images and a CT model,", IEEE/CAA J. Autom. Sin. 7 (4) (2020) 1124–1133, https://doi.org/10.1109/JAS.2019.1911528.
[24] W. Yu, M. Tannast, G. Zheng, Non-rigid free-form 2D–3D registration using a B-spline-based statistical deformation model, Pattern Recognit 63 (2017) 689–699, https://doi.org/10.1016/j.patcog.2016.09.036.
[25] T. Cresson, D. Branchaud, R. Chav, B. Godbout, J.A. De Guise, 3D shape reconstruction of bone from two x-ray images using 2D/3D non-rigid registration based on moving least-squares deformation, in: Proc. SPIE Med. Imaging, 7623, 2010, https://doi.org/10.1117/12.844098.
[26] G. Zheng, S. Gollmer, S. Schumann, X. Dong, T. Feilkas, M.A. Gonzalez Ballester, A 2D/3D correspondence building method for reconstruction of a patient-specific 3D bone surface model using point distribution models and calibrated X-ray images, Med. Image Anal. 13 (6) (2009) 883–899, https://doi.org/10.1016/j.media.2008.12.003.
[27] S. Miao, Z.J. Wang, R. Liao, A CNN regression approach for real-time 2D/3D registration, IEEE Trans. Med 35 (5) (2016) 1352–1363, https://doi.org/10.1109/TMI.2016.2521800.
[28] R. Liao, S. Miao, P. De Tournemire, S. Grbic, A. Kamen, T. Mansi, D. Comaniciu, An artificial agent for robust image registration, in: 31th AAAI Conf. Artif. Intell., vol. 31, 2017, pp. 4168–4175, https://doi.org/10.1609/aaai.v31i1.11230, 1.
[29] J. Zheng, S. Miao, Jane Wang, R. Liao, Pairwise domain adaptation module for CNN-Based 2-D/3-D registration, J. Med. Imaging 5 (2) (2018), https://doi.org/10.1117/1.JMI.5.2.021204.
[30] A. Cuno, C. Esperança, A. Oliveira, P.R. Cavalcanti, 3D as-rigid-as-possible deformation using MLS,, in: Proc. 27th Comp. Graph, Int. Conf., 2007, pp. 115–122.
[31] G. Haskins, U. Kruger, P. Yan, Deep learning in medical image registration: a survey, Mach. Vis. Appl. 31 (8) (2020) 1–18, https://doi.org/10.1007/s00138-020-01060-x.
[32] G. Balakrishnan, A. Zhao, M.R. Sabuncu, J. Guttag, A.V. Dalca, Voxelmorph: a learning framework for deformable medical image registration, IEEE Trans. Med 38 (2019) 1788–1800, https://doi.org/10.1109/TMI.2019.2897538.
[33] J. Chen, E.C. Frey, Y. He, W.P. Segars, Y. Li, Y. Du, TransMorph: transformer for medical image registration, Med. Image Anal. 82 (2022), https://doi.org/10.1016/j.media.2022.102615.
[34] Y. Kasten, D. Doktofsky, I. Kovler, End-to-End convolutional neural network for 3D reconstruction of knee bones from Bi-planar X-ray images, in: Mach. Learn. Med. Image Recons. (MLMIR), 2020, pp. 123–133, https://doi.org/10.1007/978-3-030-61598-7_12.
[35] N. Babazadeh Khameneh, C. Vazquez, T. Cresson, F. Lavoie, J.A. De Guise, Highly accurate automated patient-specific 3D bone pose and scale estimation using Bi-planar pose-invariant patches in a CNN-Based 3D/2D registration framework, in: IEEE 18th Int. Symp. Biomed. Imaging (ISBI), 2021, pp. 681–684, https://doi.org/10.1109/ISBI48211.2021.9433843.
[36] K.S. Arun, T.S. Huang, S.D. Blostein, Least-squares fitting of two 3-D point sets, IEEE Trans. Pattern Anal. Mach. Intell. 9 (5) (1987) 698–700, https://doi.org/10.1109/TPAMI.1987.4767965.
[37] R.O. Agomma, C. Vazquez, T. Cresson, J.A. De Guise, Detection and identification of lower-limb bones in biplanar X-ray images with arbitrary field of view and various patient orientations, in: *IEEE 16thInt. Symp. Biomed. Imaging (ISBI)*, 2019, pp. 1174–1177, https://doi.org/10.1109/ISBI.2019.8759456.
[38] X. Glorot, Y. Bengio, Understanding the difficulty of training deep feedforward neural networks, in: 13th Int. Conf. Artif. Intell. Stat. (PMLR), vol. 9, 2010, pp. 249–256, in: https://proceedings.mlr.press/v9/glorot10a.html.
[39] D.P. Kingma, J. Ba, Adam: a method for stochastic optimization, in: Int. Conf. Learn. Repre. (ICLR), 2015, https://doi.org/10.48550/arXiv.1412.6980.
[40] P.J. Besl, N.D. McKay, A method for registration of 3-D shapes, IEEE Trans. Pattern Anal. Mach. Intell. 14 (2) (1992) 239–256, https://doi.org/10.1109/34.121791.
[41] M.Y. Ansari, Y. Yang, S. Balakrishnan, J. Abinahed, A. Al-Ansari, M. Warfa, O. Almokdad, A. Barah, A. Omer, A.V. Singh, P.K. Meher, J. Bhadra, O. Halabi, M. F. Azampour, N. Navab, T. Wendler, S.P. Dakua, Lightweight neural network with multiscale feature enhancement for liver CT segmentation," *scientific reports*, Nature 12 (14153) (2022), https://doi.org/10.1038/s41598-022-16828-6.
[42] M.Y. Ansari, Y. Yang, P.K. Meher, S.P. Dakua, Dense-PSP-UNet: a neural network for fast inference liver ultrasound segmentation, Comput. Biol. Med. 153 (2023) 106478, https://doi.org/10.1016/j.compbiomed.2022.106478.
[43] P. Jannin, J.M. Fitzpatrick, D.J. Hawkes, X. Pennec, R. Shahidi, M.W. Vannier, Validation of medical image processing in image-guided therapy, IEEE Trans. Med 21 (12) (2002) 1445–1449, https://doi.org/10.1109/TMI.2002.806568. *Image*.
[44] S.D. Roth, Ray casting for modeling solids, Comput. Graph. Image Process. 18 (1982) 109–144, https://doi.org/10.1016/0146-664X(82)90169-1.
[45] J. Salvi, C. Matabosch, D. Fofi, J. Forest, A review of recent range image registration methods with accuracy evaluation, Image Vis Comput. 25 (5) (2007) 578–596, https://doi.org/10.1016/j.imavis.2006.05.012.
[46] J. Yao, Taylor, Assessing accuracy factors in deformable 2D/3D medical image registration using a statistical pelvis model, in: IEEE 9th Int. Conf. Comp. Visio. (ICCV), vol. 2, 2003, pp. 1329–1334, https://doi.org/10.1109/ICCV.2003.1238644.